RSC Advances

ROYAL SOCIETY OF CHEMISTRY

www.rsc.org/advances

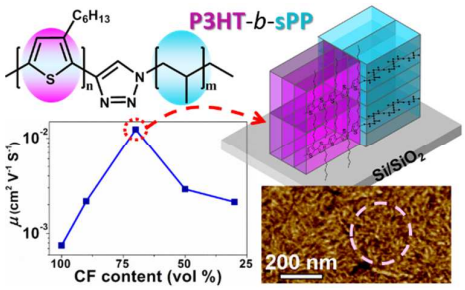

Molecular Stacking Structure and Field-Effect Transistor Characteristics of Crystalline Poly(3-hexylthiophene)-*block*-Syndiotactic Polypropylene through Solvent Selectivity

Chen-Tsyr Lo,[1] Chih-Jung Lin,[1] Jing-Yu Lee,[2] Shih-Huang Tung,[3]

Jing-Cherng Tsai,[2,] and Wen-Chang Chen[1,]**

[1]Department of Chemical Engineering, National Taiwan University, Taipei 10617, Taiwan.

[2]Department of Chemical Engineering, National Chung Cheng University, Chia-Yi 62142, Taiwan.

[3]Institute of Polymer Science and Engineering, National Taiwan University, Taipei 10617, Taiwan

*Author to whom all correspondence should be addressed: chenwc@ntu.edu.tw (W. C. Chen); chmjct@ccu.edu.tw (J. C. Tsai)

Abstract

We investigate the molecular packing structures, morphologies and field-effect characteristics of the crystalline-crystalline poly(3-hexylthiophene)-*block*-syndiotactic polypropylene block copolymers (P3HT-*b*-sPP) using different solvent mixtures of chloroform/cyclohexane (CF/CH). For the P3HT-*b*-sPP with a shorter sPP segment length, the increase of CH solvent content led to the P3HT domain with highly crystalline nanofibrillar networks and thus improved the charge transporting characteristics. For the P3HT-*b*-sPPs with a longer sPP segment length, well-defined microstructure and device characteristics were only observed at the 70 vol% CF content. Furthermore, the self-encapsulation of the insulating sPP blocks effectively improved the air stability of the P3HT-*b*-sPP field transistor devices. This work highlights the significance of solvent selectivity and rod/coil block ratios on the molecular packing and the organic field-effect transistor performances.

Keywords

rod-coil block copolymers, P3HT, field effect transistor, solvent effect, crystallinity

1. Introduction

Conjugated rod-coil block copolymers have received extensive research interest because they offer a systematic route towards materials with novel architectures, functions and physical properties.[1-6] With the additional structural control parameters provided by the conjugated rod, the block copolymer can generate multiple nanoscale morphologies and molecular organization, resulting in well-defined electronic and optoelectronic properties.

Regioregular P3HT is one of the most explored solution-processable conjugated polymers for electronic and optoelectronic applications due to the excellent charge-transporting properties. By incorporating a non-conjugated coil block into P3HT, the formation of ordered nanostructures from the block copolymer could further improve the electrical properties of organic field effect transistor (OFET) devices.[7-19] In addition, these P3HT-coil block copolymers feature one economical solution as well as prominent mechanical properties and environmental stability that are prerequisites for device applications.[5,7,20] On the other hand, crystalline-crystalline block copolymers provide an additional pathway to tune the molecular self-organization,[14,15,17,19-29] which were resulted from the interplay between crystallization and microphase-separation. It has been shown that the well-oriented crystalline structures of block copolymers may be obtained from the lattice matching effect near the interface of two structural similar crystals.[27-31] The morphological

transformation in thin films of conjugated rod-coil block copolymers were governed by several driving forces, such as the rod/coil ratio and mixed solvent composition.[1,2,5] We reported crystalline-crystalline poly(3-hexylthiophene)-*block*-syndiotactic polypropylene (P3HT-*b*-sPP) and correlated the rod/coil ratios with field-effect characteristics.[19] The sPP block with an adequate length significantly enhanced the molecular packing of P3HT domain and further improved the FET mobility. However, the solvent selectivity effect on the molecular stacking structures and FET characteristics of crystalline block copolymers have not been fully explored yet.

In this study, the effect of solvent selectivity on the thin film morphology and resulted electronic properties of P3HT-*b*-sPP was studied using the solvent mixtures of chloroform/cyclohexane (CF/CH). The chemical structures of the two studied block copolymers, $P3HT_{16K}$-*b*-sPP_{3K} (P1) and $P3HT_{16K}$-*b*-sPP_{14K} (P2), are shown in Figure 1. The CF is a good solvent for P3HT but a marginal solvent for sPP; in contrast, CH is a marginal solvent for P3HT but a good solvent for sPP. The morphology was characterized using grazing incidence wide angle X-ray scattering (GIWAXS), atomic force microscopy (AFM), transmission electron microscopy (TEM). The photophysical properties were investigated using UV-Vis absorption spectra. OFET devices were fabricated from P3HT-*b*-sPP using the bottom-gate top-contact configuration. The experimental results suggested that both the CF-CH

solvent composition and the rod/coil block ratio could effectively control the molecular packing of P3HT-*b*-sPP and the resulted FET characteristics.

2. Experimental Section

Materials

Synthesis and characterization of P3HT-*b*-sPP diblock copolymers were reported previously.[19] The P3HT-*b*-sPPs were prepared with different sPP segment lengths, i.e. $P3HT_{16K}$-*b*-sPP_{3K} (P1) and $P3HT_{16K}$-*b*-sPP_{14K} (P2), which had the regioregularity of the P3HT block of 97.5% (Figure S1, ESI†) and 97.7% (Figure S2, ESI†), respectively. P3HT homopolymer (M_w ~ 28,000 g mol^{-1}, regioregularity: 95 %) was supplied by Rieke Metals Inc., USA. Common organic solvents for rinsing wafers, such as toluene, acetone, and isopropyl alcohol (IPA), were purchased from TEDIA, USA. Ultra-anhydrous solvents for device applications, such as chloroform (CF, ≥99%) and cyclohexane (CH, 99.5%), were obtained from Sigma-Aldrich, USA.

Thin-Film Preparation and Characterization

The block copolymer solution with the concentration of 3 mg mL^{-1} was prepared using the chloroform(CF)-cyclohexane(CH) solvent mixtures with the compositions of 100, 90, 70, 50, and 30 vol % of CF, respectively. In order to make sure that the polymers were completely dissolved, all solutions were first heated to 40 °C for 1 h

and then cooled at room temperature. Polymer thin films were spin-coated at 600 rpm for 60 sec onto substrates in a N_2-filled glove box and vacuum-dried for 8 h. Thin films were thus prepared on glass slides for UV-Vis measurement and on bare SiO_2/Si substrates for the characterization of GIWAXS, AFM, and OFET. Prior to spin-coating, the substrates were rinsed with toluene, acetone, and IPA in sequence.

UV-Vis absorption spectra were measured with Hitachi U4100 spectrophotometer. GIWAXS patterns were recorded from Rigaku Nano Viewer. The incident angle and scan range of GIWAXS measurement were 0.23° and 2-30°, respectively. The surface structures of thin films were studied using Digital Instruments AFM with a Nanoscope 3D Controller operated in the tapping mode at room temperature. TEM images were obtained using JOEL JEM-1230, operated at 100 kV, equipped with a Gatan DualVision CCD. Samples for the TEM characterization were prepared by spin-coating at 600 rpm for 60 s onto carbon-coated copper grids.

Device Fabrication and Measurement

OFET devices were fabricated in a bottom-gate top-contact configuration using the heavily doped (n^{++}) silicon (100) wafer as the substrate and a thermally grown 300 nm SiO_2 layer as the gate insulator. 100-nm-thick Au source and drain electrodes were deposited through a regular shadow mask, with the channel length (L) and width (W)

were 50 and 1000 μm, respectively. Electronic characterization of the OFET device was studied using a Keithley 4200 semiconductor parametric analyzer. Device fabrication and all electrical measurements were performed in a N_2 atmosphere; otherwise, the devices were stored in air (humidity level: 50-60 %). Field-effect mobilities (μ) were extracted from the saturated transfer characteristics employing the relation: $I_{ds} = \mu(WC/2L)(V_{gs} - V_t)^2$, where I_{ds} is the souce-drain current, V_{gs} and V_t gate and threshold voltage, respectively, C the capacitance of gate insulator, W and L the channel width and length.

3. Results and Discussions

3.1. Optical Properties

Figure 2 shows the UV-Vis absorption spectra of the P3HT-*b*-sPP and P3HT thin films, prepared from different solvent mixtures of CF/CH. The absorption bands with the maximum absorption wavelengths at 525 (shoulder), 555 (λ_{max}), and 605 (shoulder) nm are clearly observed in all the spectra, which are typical characteristic bands of highly ordered P3HT chains.[32,33] As shown in the spectra, P1 (Figure 2a) with the shorter sPP block length, exhibits a similar trend with P3HT (Figure 2c). Reducing the CF solvent content apparently red-shifts the position of the maximum adsorption wavelength from 555 to 565 nm. In addition, the shoulder in the lower energy region

($\lambda_{\pi\text{-}\pi}$, λ = 605 nm) exhibits a fairly stronger intensity as the CF content is decreased, which is attributed to the interchain exciton delocalization across the ordered P3HT π-π stacking chains.[32,33] It suggests that the marginal solvent CH could improve the molecular stacking of the P3HT chain in the P3HT-*b*-sPP.[32, 33] However, the development of P3HT π-π stacking may be restrained by an excessively longer sPP segment and thus results in reduced absorption coefficients in the spectra. For the case of P2 (Figure 2b) with the longer sPP segment, the absorption coefficient initially increases but reduces as the CF content is lower than 70 vol%. CH is known as a marginal solvent for P3HT but a good solvent for sPP. Thus, the long sPP segment could hinder the P3HT stacking under the CH-rich conditions (i.e. CF content is 50 and 30 vol%) and it explains the trend on the P2 absorption spectra in different solvent mixtures.

Figure 3 shows the absorption spectra of P3HT and P3HT-*b*-sPP thin films prepared from three different solvent compositions. With the 100 vol% CF solvent (Figure 3a), the P1 spectrum shows higher adsorption coefficients than that of P3HT film, indicating the enhanced P3HT chain stacking after incorporating the sPP block. However, the absorption coefficient reduces in the spectra of P2 with a longer sPP block length, attributed to the hindrance of P3HT chain packing. In the 70 vol% CF solvent mixture (Figure 3b), both P1 and P2 spectra exhibit higher adsorption

coefficients than that of the P3HT film, suggesting the formation of ordered P3HT packing structure.[33] However, the trend on the absorption spectra using the 30 vol% CF solvent mixture (Figure 3c) is similar to that with 100 vol% CF. One interesting feature is that, though the P2 spectra show suppressed adsorption coefficients in 100 or 30 vol% CF solvent, a relatively large adsorption coefficient is observed for the P2 spectrum with the 70 vol% CF solvent mixture. The above result suggests that both the CF-CH solvent composition and the sPP segment length significantly affect the interchain interaction and effective conjugation length of the P3HT-*b*-sPP films, which will correlate with the morphology and field-effect characteristics as follows.

3.2. Molecular Stacking Structure

GIWAXS was used to investigate the molecular organization of P3HT-*b*-sPP via varying the CF/CH ratio. Figure 4 shows the GIWAXS patterns of the P1 and P2 thin films prepared from three different CF/CH solvent compositions, i.e. 100/0, 70/30, and 30/70 (vol%), while those of P3HT are shown in Figure S3 (ESI†). Evident P3HT out-of-plane lamellar-layer structure, i.e. (100) and (200) along the q_z direction and π-π interchain stacking (010) along the q_{xy} direction, is observed in all the GIWAXS patterns, with a spacing of 16.20 Å for P3HT lamella and 3.82 Å for π-π stacking.[34-38] For the case of P1 with the shorter sPP segment (Figure 4a), it exhibits a significantly improved ordering on P3HT lamellar stacking, i.e. (100), (200), and (300) diffractions

can be clearly seen, when compared to that of P3HT (Figure S3, ESI†). With the decreased CF solvent content, the P1 film shows narrower diffraction arcs, particularly for the case of 30 vol% CF (Figure 4a-(iii)), which implies a more oriented P3HT lamellae stacking lying on the substrate. In contrast, the diffraction of the sPP crystalline domains in P1 is weak because of the low sPP fraction and also, the aggregation of the long P3HT chain may constrain the short sPP chain from a regular arrangement. The diffraction arcs of sPP (020) is vaguely seen, with a d-spacing ~ 5.61 Å identical to that reported by Lotz and Lovinger.[39]

The GIWAXS patterns of P2 with the longer sPP block are shown in Figure 4b. The diffraction arcs of the sPP crystalline domains are more pronounced compared to those of P1. In addition to the (020) plane, the diffraction of the sPP (200) plane with a d-spacing of 7.23 Å can be clearly seen and appear dominantly at the q_{xy} axis. The diffraction arcs of the sPP (220) plane are also observed at azimuthal angles between q_{xy} and q_z axes.[39] Such diffraction patters suggest that sPP chain axis tends to be parallel to the substrate and form an edge-on alignment of the sPP crystalline lamellae relative to the substrate. Compared to P1, the P2 with the longer sPP chain apparently makes a negative impact on the packing of P3HT. Although the strong diffraction of P3HT at the q_z axis is still observed, the higher order peaks are diminished. It indicates that the stacking of P3HT lamellae on the substrate is not as regular as that

of P1. Furthermore, the diffraction on the π-π interchain stacking (010) is nearly undetectable for P2. The lateral packing of P3HT chains is deteriorated by the long sPP chain as well. For the case of 70 vol% CF (Figure 4b-(ii)), the diffractions of sPP are relatively sharp and the intensity of (200) is much stronger than that of (020) along the q_{xy} axis. It suggests a more regular and oriented packing of the sPP chains with the *a*-axis direction of the sPP crystalline lamella parallel to the substrate. The diffraction of the P3HT block in P2 is also shaper than that of others, implying a more oriented P3HT lamella lying on the substrate for 70 vol% CF.

3.3. Morphology

The Flory-Huggins interaction parameter, χ, is generally employed to predict the compatibility in polymer solutions.[41] The $\chi_{polymer\text{-}solvent}$ values listed in Table S2 (ESI†) are the interaction parameter between the assigned polymer block and the solvent. The $\chi_{sPP\text{-}solvent}$ values of the CF-rich solvent conditions (0.394 for 100 vol % and 0.356 for 90 vol %) are much higher than the corresponding $\chi_{P3HT\text{-}solvent}$ values (0.031 for 100 vol % and 0.048 for 90 vol %). This suggests that sPP block has a higher incompatibility with the solvents and tend to aggregate in the solution, resulting in a higher crystallization driving force of sPP when compared to P3HT during thin film casting process. The addition of the sPP-selective CH in the solvent can tune the crystallization rate and the microphase-separation behavior of the two blocks, which

affects the molecular packing of P3HT-*b*-sPP.

The AFM and TEM images of the P1 and P2 thin films prepared with different CF/CH ratios are shown in Figure 5, where the dark regions in the TEM images can be directly related to the P3HT domain due to its higher electron density. For the P1 with the shorter sPP segment length, a well-defined P3HT nanofibrillar structure is observed in thin films prepared from pure CF ((i)-(iv) in Figure 5. It suggests that the pre-formed crystals of the shorter sPP blocks would not hinder the packing of the P3HT blocks. Instead, the microphase separation provides a distinct P3HT-sPP interface along which P3HT blocks can pack more regularly to form nanofibers with significantly improved ordering as evidenced in the GIWAXS pattern (Figure 4a). As the CF solvent content is gradually decreased, the P3HT blocks tend to aggregate and the driving force for the P3HT crystallization becomes stronger. Therefore, well packed P3HT chains form thicker and continuous structures as shown in (ii)-(iii) of Figure 5a and (v)-(vi) of Figure 5a, which could facilitate the transport of charge carriers.

The effect of the solvent selectivity on the morphology of the P2 with the longer sPP segment is different from that of P1. As shown in (i)-(iv) of Figure 5b, the structures are dominated by the large crystals of sPP blocks, where only a small amount of P3HT crystals is observed. Due to the high crystallization driving forces of

the long sPP chains in CF, the pre-formed sPP crystals suppress the mobility of polymer chains toward microphase separation so that P3HT chains are unable to pack in a regular manner.[40] It is interesting that uniform P3HT nanofibers are observed when the CF content in solvent reduces to 70 vol %, as shown in (ii)-(v) of Figure 5b. At this solvent composition, the difference between the $\chi_{sPP\text{-}solvent}$ and $\chi_{P3HT\text{-}solvent}$ values is reduced, indicating the difference in crystallization driving force between sPP and P3HT is not as high as that in pure CF. The decreased crystallization driving force of sPP probably allows the microphase separation to occur prior to crystallization of both blocks and P3HT chains can then pack more orderly in the well-defined microdomains. However, when the CF solvent content is further reduced to 30 vol% shown in (iii)-(vi) of Figure 5b, P3HT domains become discontinuous and isolated spherical P3HT regions appear. With a high CH content, P3HT-*b*-sPP may form spherical micelles in the solution where P3HT aggregates in the core stabilized by long sPP chains in the corona. When cast into thin films, the micelle structures are retained after solvent evaporates, thus causing the formation of the isolated P3HT domains separated by sPP phases in thin films. The enhanced aggregation and crystallization driving forces of P3HT are also supported by the values of $\chi_{sPP\text{-}solvent}$ and $\chi_{P3HT\text{-}solvent}$ in the CF-poor solvent composition (selective to sPP block), which are 0.146 and 0.262, respectively. Moreover, we conducted SAXS measurements on

the P3HT-*b*-sPP diblock copolymers after solvent evaporation. The representative data of P1 sample prepared from pure chloroform (CF) without further annealing is shown in Figure S4 (ESI†). Although the lacking of clear diffraction peaks for the highly ordered structure, a shoulder at $Q \sim 0.03$ Å^{-1} corresponding to a characteristic length of 21 nm reveals the approximate scale of the microdomains. The morphological results based on the TEM images and the additional information from SAXS analyses suggest the tendency of P3HT-*b*-sPPs to microphase separate into microdomains. Also, the above results show that the solvent selectivity has a significant effect on the balance between the crystallization and the microphase separation of block copolymers.

3.4. Characteristics of Field-Effect Transistors

The electrical characteristics of the P3HT-*b*-sPP based OFET devices are listed in Table 1, where the P3HT characteristics are also included for comparison. The average data of OFET performance are obtained from at least 10 devices of two batches. All FET devices exhibit good current modulation and well-defined saturation regions as shown in the represented transfer and output characteristics of the P2 device in Figure 6. The field-effect mobilities with different solvent composition are further illustrated in Figure 7. For the P1 device, the mobility is enhanced from 4.15×10^{-3} to 1.34×10^{-2} $cm^2V^{-1}s^{-1}$ as the CH solvent content is increased. It confirms the

orderly packing of the P3HT chains in the case of the short sPP chains. However, the FET mobility of the P2 thin film obtained from pure CF is relatively low, 7.53×10^{-4} $cm^2V^{-1}s^{-1}$, due to the stronger crystallization driving force of sPP that hinders P3HT chains from regular packing. As the CF content is decreased to 70 vol%, the P2 device shows the highest mobility of 1.24×10^{-2} $cm^2 V^{-1} s^{-1}$. It suggests that the addition of 30 vol% of CH in solvent provides a balance between crystallization and microphase separation that leads to the formation of the ordered P3HT microstructure for the obtained high field-effect mobility. As the CF solvent content is further reduced to 50 and 30 vol%, the field-effect mobility is decreased again. As the morphology shown in (iii)(vi) of Figure 5b, the tendency of the P3HT block in P2 to form aggregates surrounded by the long sPP chains in CH-rich solvents. It leads to the discontinuous P3HT microphase-separated domains and hence the mobility is suppressed. The above result indicates that both the CF-CH solvent composition and the sPP segment length can significantly affect the performance of P3HT-*b*-sPP OFET devices.

3.5. Environmental Stability

The air stability on the P3HT-*b*-sPP and P3HT OFET devices shown in Figure 8 was obtained by measuring the field effect mobility (μ), on-off ratio, and threshold voltage (V_t) as a function of time in air. These thin films were prepared from the 70

vol% CF solvent. In contrast to the dramatic degradation in the mobility of the P3HT device within 240 h, all P3HT-*b*-sPP OFET devices exhibit a significantly improved air stability. After being stored in air for about two months, all the carrier mobilities of the P1 and P2 devices are sustained at similar values, while the P3HT FET exhibits a nearly 75% degradation. Moreover, while the P3HT device shows a considerable reduction in the on-off ratio with increasing the storage time, the on-off ratios of the P1 and P2 devices increase slightly to 10^5 due to the reduced OFF currents. It could be attributed to the suppression of the leakage current resulted from the residual oxygen or moisture desorption in the devices. Furthermore, the threshold voltages of the P2 devices are slightly shifted 5-8 V after being stored in air for two months, indicating the excellent oxidative resistance in air. Compared to the P3HT OFET device, the air stable P3HT-*b*-sPP OFET devices can be attributed to the self-encapsulation effect resulted from the insulating sPP layer covering the surface of the active P3HT channel to prevent oxygen and moisture from ambient.[5,8,20]

4. Conclusions

We have investigated the effects of both the solvent selectivity and rod/coil ratio on the molecular packing structures, morphologies and field-effect characteristics of the crystalline-crystalline P3HT-*b*-sPP diblock copolymers. The effects of the mixed solvent composition on the morphology of P3HT-*b*-sPP are significantly different for

various sPP segment lengths. For P3HT-*b*-sPP with the short sPP chain, the sPP crystallization does not affect the P3HT packing, and thus the P3HT block form continuous well-defined microdomains for high field-effect mobility. On the other hand, For P3HT-*b*-sPP with the long sPP chain, the interplay between each block and solvent composition is more complicated and the field-effect mobility reaches a maximum at a specific CF/CH solvent composition. The large fraction of sPP pre-formed crystals formed in the solvent mixture may inevitably hinder the packing of P3HT. Also, due to the large volume fraction of sPP, the P3HT microdomains may be separated by the sPP phases and become a discontinuous structure. As a result, the microphase-separation behaviors and the crystallization driving force of each block in solvent mixtures significantly affect the resulting microstructures in P3HT-*b*-sPP thin film with the long sPP block. In addition, the effective self-encapsulation of the insulating sPP blocks on P3HT channels can significantly improve air stability of the P3HT-*b*-sPP OFET devices. This study provides a guideline for improving the performance of field-effect transistors via solvent selectivity on crystalline conjugated rod-coil block copolymers.

Acknowledgement

The financial support from National Science Council of Taiwan and National Taiwan

TOP University Research program are greatly appreciated.

Supporting Information

† Electronic Supplementary Information (ESI) available: detailed sample information, calculated results of Flory-Huggins interaction parameters (χ) and GIWAXS patterns of P3HT are provided in this section.

References

(1) C. L. Liu, C. H. Lin, C. C. Kuo, S. T. Lin and W. C. Chen, *Prog. Polym. Sci.*, 2011, **36**, 603-637.

(2) P. Leclère, E. Hennebicq, A. Calderone, P. Brocorens, A. C. Grimsdale, K. Müllen, J. L. Brédas and R. Lazzaroni, *Prog. Polym. Sci.*, 2003, **28**, 55-81.

(3) F. J. M. Hoeben, P. Jonkheijm, E. W. Meijer and A. P. H. J. Schenning, *Chem. Rev.*, 2005, **105**, 1491-1546.

(4) Y. Liang, H. Wang, S. Yuan, Y. Lee, L. Gan and L. Yu, *J. Mater. Chem.*, 2007, **17**, 2183-2194.

(5) B. D. Olsen and R. A. Segalman, *Mater. Sci. Eng. R: Rep.*, 2008, **62**, 37-66.

(6) D. Haynes, M. C. Stefan, R. D. McCullough, Conjugated–Insulating Block Copolymers: Synthesis, Morphology, and Electronic Properties. In *Semiconducting*

Polymer Composites; Wiley-VCH Verlag GmbH & Co. KGaA: Weinheim, 2012, pp. 299-330.

(7) X. Yu, K. Xiao, J. Chen, N. V. Lavrik, K. Hong, B. G. Sumpter and D. B. Geohegan, *ACS Nano*, 2011, **5**, 3559-3567.

(8) J. Liu, D. Haynes, C. Balliet, R. Zhang, T. Kowalewski and R. D. McCullough, *Adv. Funct. Mater.*, 2012, **22**, 1024-1032.

(9) C. Renaud, S. J. Mougnier, E. Pavlopoulou, C. Brochon, G. Fleury, D. Deribew, G. Portale, E. Cloutet, S. Chambon, L. Vignau and G. Hadziioannou, *Adv. Mater.*, 2012, **24**, 2196-2201.

(10) G. Sauvé and R. D. McCullough, *Adv. Mater.*, 2007, **19**, 1822-1825.

(11) S. Y. Choi, J. U. Lee, J. W. Lee, S. Lee, Y. J. Song, W. H. Jo and S. H. Kim, *Macromolecules*, 2011, **44**, 1771-1774.

(12) M. Arif, J. Liu, L. Zhai, S. I. Khondaker, *Synth. Met.*, 2012, **162**, 1531-1536.

(13) Y. J. Lee, S. H. Kim, H. Yang, M. Jang, S. S. Hwang, H. S. Lee and K. Y. Baek, *J. Phys. Chem. C*, 2011, **115**, 4228-4234.

(14) C. Müller, S. Goffri, D. W. Breiby, J. W. Andreasen, H. D. Chanzy, R. A. J. Janssen, M. M. Nielsen, C. P. Radano, H. Sirringhaus, P. Smith and N. Stingelin-Stutzmann, *Adv. Funct. Mater.*, 2007, **17**, 2674-2679.

(15) A. Kumar, M. A. Baklar, K. Scott, T. Kreouzis, N. Stingelin-Stutzmann, *Adv.*

Mater., 2009, **21**, 4447-4451.

(16) J. C. Lin, W. Y. Lee, C. C. Kuo, C. Li, R. Mezzenga and W. C. Chen, *J. Polym. Sci. Part A: Polym. Chem.*, 2012, **50**, 686-695.

(17) V. Ho, B. W. Boudouris, B. L. McCulloch, C. G. Shuttle, M. Burkhardt, M. L. Chabinyc and R. A. Segalman, *J. AM. CHEM. SOC.*, 2011, **133**, 9270-9273.

(18) M. G. Alemseghed, S. Gowrisanker, J. Servello and M. C. Stefan, *Macromol. Chem. Phys.*, 2009, **210**, 2007-2014.

(19) J. Y. Lee, C. J. Lin, C. T. Lo, J. C. Tsai and W. C. Chen, *Macromolecules*, 2013, **46**, 3005-3014.

(20) B. D. Olsen, X. Li, J. Wang and R. A. Segalman, *Macromolecules*, 2007, **40**, 3287-3295.

(21) C. P. Radano, O. A. Scherman, N. Stingelin-Stutzmann, C. Müller, D. W. Breiby, P. Smith, R. A. J. Janssen and E. W. Meijer, *J. AM. CHEM. SOC.*, 2005, **127**, 12502-12503.

(22) B. W. Boudouris, C. D. Frisbie and M. A. Hillmyer, *Macromolecules*, 2008, **41**, 67-75.

(23) G. Grancharov, O. Coulembier, M. Surin, R. Lazzaroni and P. Dubois, *Macromolecules*, 2010, **43**, 8957-8964.

(24) A. C. Kamps, M. Fryd and S. J. Park, *ACS Nano*, 2012, **6**, 2844-2852.

(25) I. Botiz, A. B. F. Martinson and S. B. Darling, *Langmuir*, 2010, **26**, 8756-8761.

(26) I. Botiz and S. B. Darling, *Macromolecules*, 2009, **42**, 8211-8217.

(27) C. De Rosa, C. Park, E. L. Thomas and B. Lotz, *Nature*, 2000, **405**, 433-437.

(28) R. M. Ho, P. Y. Hsieh, W. H. Tseng, C. C. Lin, B. H. Huang and B. Lotz, *Macromolecules*, 2003, **36,** 9085-9092.

(29) C. De Rosa, C. Park, B. Lotz, J. C. Wittmann, L. J. Fetters and E. L. Thomas, *Macromolecules*, 2000, **33**, 4871-4876.

(30) J. C. Wittmann and B. Lotz, *J. Polym. Sci., Polym. Phys. Ed.*, 1981, ***1837***.

(31) J. C. Wittmann and B. Lotz, *J. Polym. Sci., Polym. Phys. Ed.*, 1981, ***1853***.

(32) A. Salleo, R. J. Kline, D. M. DeLongchamp and M. L. Chabinyc, *Adv. Mater.*, 2010, **22**, 3812-3838.

(33) Y. Kim, S. Cook, S. M. Tuladhar, S. A. Choulis, J. Nelson, J. R. Durrant, D. D. C. Bradley, M. Giles, I. McCulloch, C. S. Ha and M. Ree, *Nat. Mater.*, 2006, **5**, 197-203.

(34) H. Sirringhaus, P. J. Brown, R. H. Friend, M. M. Nielsen, K. Bechgaard, B. M .W. Langeveld-Voss, A. J. H. Spiering, R .A. J. Janssen, E. W. Meijer, P. Herwig and D. W. de Leeuw, *Nature*, 1999, **401**, 685-688.

(35) D. M. DeLongchamp, R. J. Kline, D. A. Fischer, L. J. Richter and M. F. Toney, *Adv. Mater.*, 2011, **23**, 319-337.

(36) R. Joseph Kline, M. D. McGehee and M. F. Toney, *Nat. Mater.*, 2006, **5**, 222-228.

(37) S. Nagamatsu, W. Takashima, K. Kaneto, Y. Yoshida, N. Tanigaki, K. Yase and K. Omote, *Macromolecules*, 2003, **36**, 5252-5257.

(38) L. H. Jimison, M. F. Toney, I. McCulloch, M. Heeney and A. Salleo, *Adv. Mater.*, 2009, **21**, 1568-1572.

(39) B. Lotz, A. J. Lovinger and R. E. Cais, *Macromolecules* 1988, **21**, 2375-2382.

(40) W. N. He and J. T. Xu, *Prog. Polym. Sci.*, 2012, **37**, 1350-1400.

(41) D. Pospiech, A. Gottwald, D. Jehnichen, P. Friedel, A. John, C. Harnisch, D. Voigt, G. Khimich and A. Bilibin, *Colloid. Polym. Sci.*, 2002, **280**, 1027-1037.

Figure Captions

Figure 1. Chemical structures of the studied P3HT-*b*-sPP, P1 and P2.

Figure 2. Absorption spectra of (a) P1, (b) P2, and (c) P3HT thin films prepared from polymer solutions with different CF content (vol%).

Figure 3. Absorption spectra of P3HT-*b*-sPP thin films prepared from polymer solutions with different CF content (vol%): (a) 100, (b) 70, and (c) 30.

Figure 4. Two-dimensional GIWAXS patterns of P3HT-*b*-sPP thin films prepared from polymer solutions with different CF content (vol%): (a) P1, (b) P2.

Figure 5. AFM and TEM images of (a) P1 (b) P2 thin films prepared from different CF solvent mixtures: (i)-(iii) AFM and (iv)-(vi) TEM.

Figure 6. (a) Transfer characteristics of the OFET devices fabricated from P2 with different CF content (vol%). (b) Output characteristics of transistor of P2 thin film prepared with 70 vol% CF.

Figure 7. Performance of the P3HT and P3HT-*b*-sPPs OFET devices with different CF content (vol%).

Figure 8. Environmental stability of the P3HT-*b*-sPP and P3HT OFET devices prepared from the 70 vol% CF solvent mixture: hole mobility (μ), on/off ratio, and threshold voltage (V_t).

Table 1. Characteristics of P3HT-*b*-sPP and P3HT OFET devices using the solvent mixtures with different CF contents (vol%).

Polymer	CF contents (vol %)	μ^{avg} ($cm^2 V^{-1} s^{-1}$)	On/off ratio	V_{th} (V)
P1	100	$(4.15 \pm 0.41) \times 10^{-3}$	2.40×10^4	13.36 ± 0.80
	90	$(3.94 \pm 0.67) \times 10^{-3}$	1.77×10^4	2.69 ± 1.90
	70	$(1.57 \pm 0.25) \times 10^{-2}$	9.39×10^4	5.32 ± 4.79
	50	$(1.70 \pm 0.13) \times 10^{-2}$	4.57×10^4	10.17 ± 5.40
	30	$(1.34 \pm 0.09) \times 10^{-2}$	7.53×10^4	10.55 ± 1.17
P2	100	$(7.53 \pm 1.57) \times 10^{-4}$	6.35×10^4	5.03 ± 8.82
	90	$(2.17 \pm 0.84) \times 10^{-3}$	1.84×10^4	1.44 ± 2.52
	70	$(1.24 \pm 0.52) \times 10^{-2}$	1.36×10^4	0.65 ± 2.51
	50	$(2.90 \pm 0.48) \times 10^{-3}$	1.04×10^4	5.65 ± 2.16
	30	$(2.13 \pm 0.53) \times 10^{-3}$	3.83×10^4	4.70 ± 0.87
P3HT	100	$(2.49 \pm 0.32) \times 10^{-3}$	4.96×10^4	2.39 ± 10.58
	90	$(1.87 \pm 0.61) \times 10^{-3}$	2.80×10^4	8.15 ± 2.09
	70	$(3.19 \pm 0.79) \times 10^{-3}$	1.15×10^4	-4.91 ± 1.04
	50	$(4.43 \pm 0.59) \times 10^{-3}$	1.06×10^4	-2.56 ± 3.98
	30	$(6.63 \pm 0.14) \times 10^{-3}$	9.15×10^3	-5.53 ± 0.76

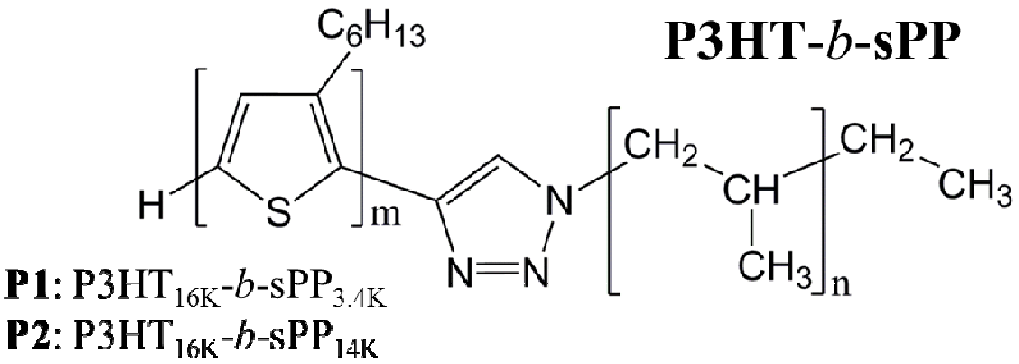

Figure 1.

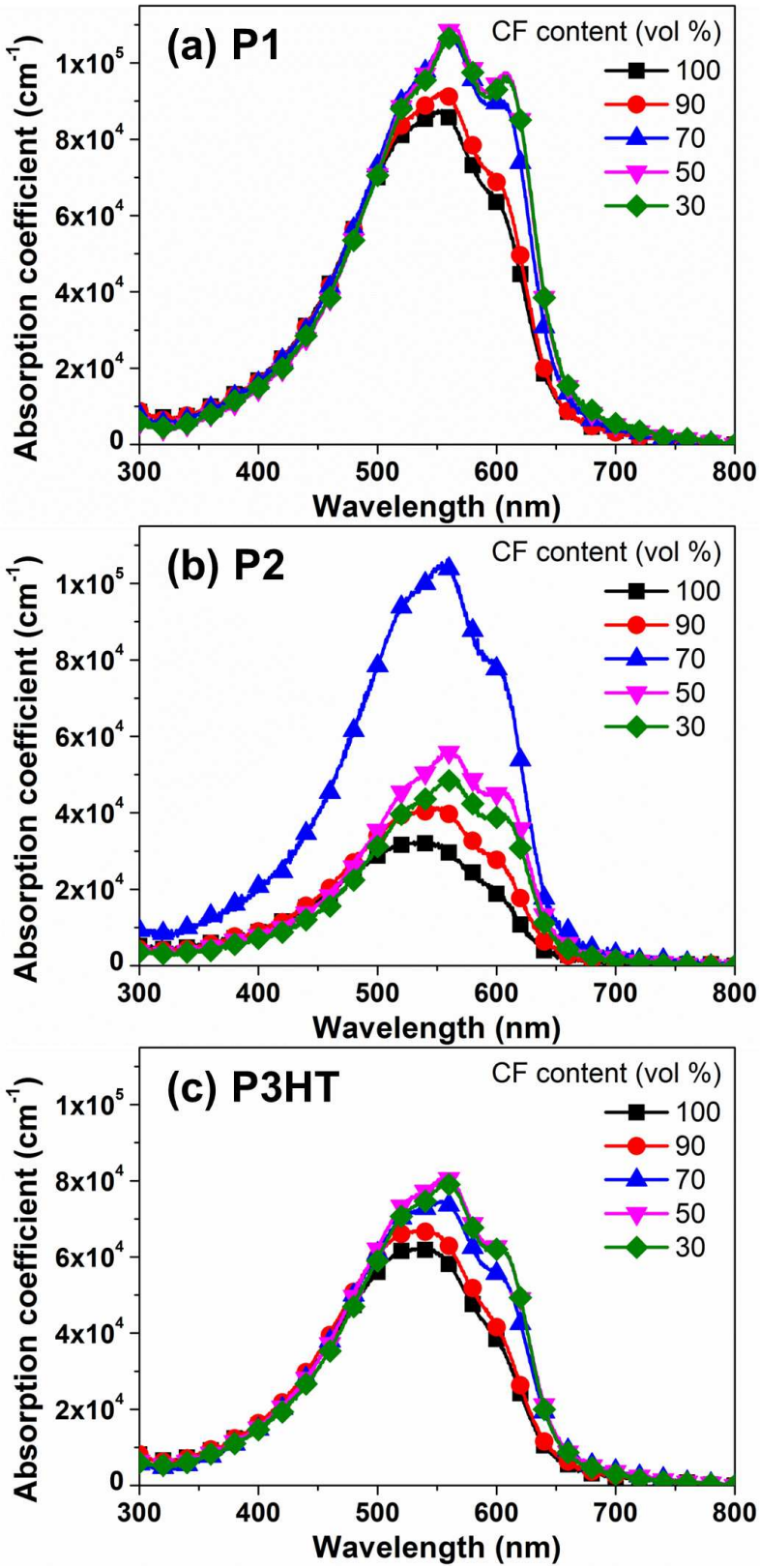

Figure 2.

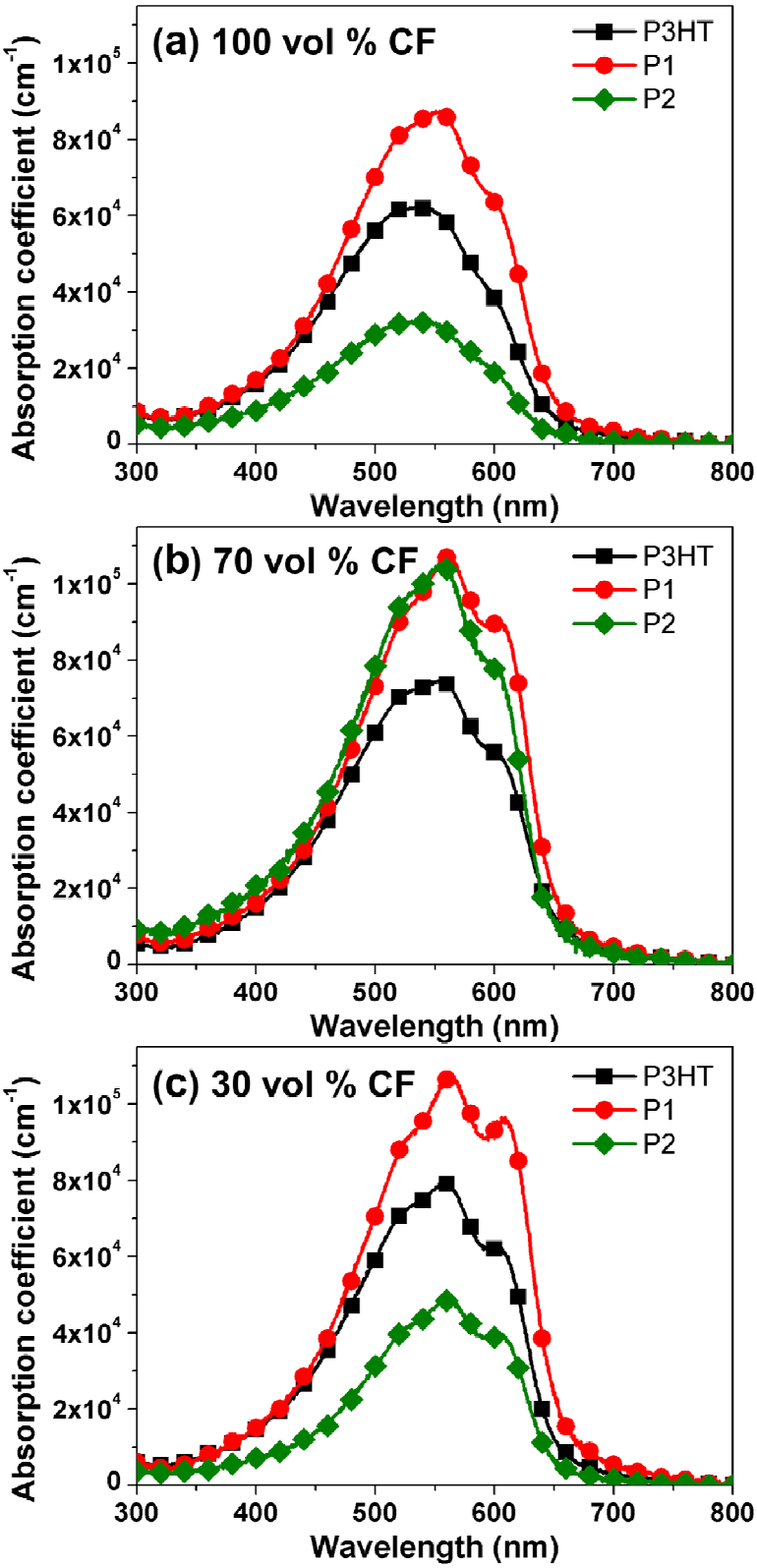

Figure 3

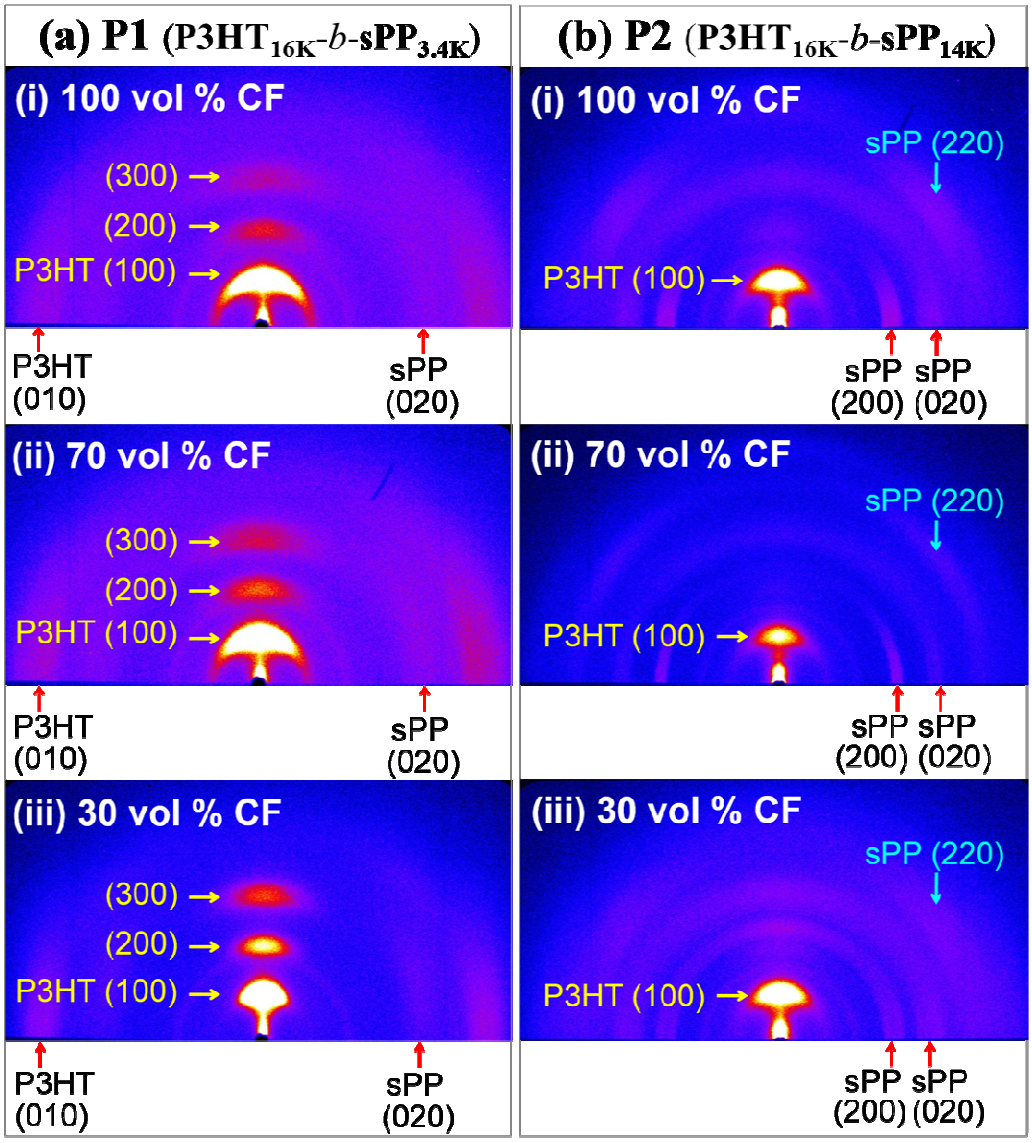

Figure 4.

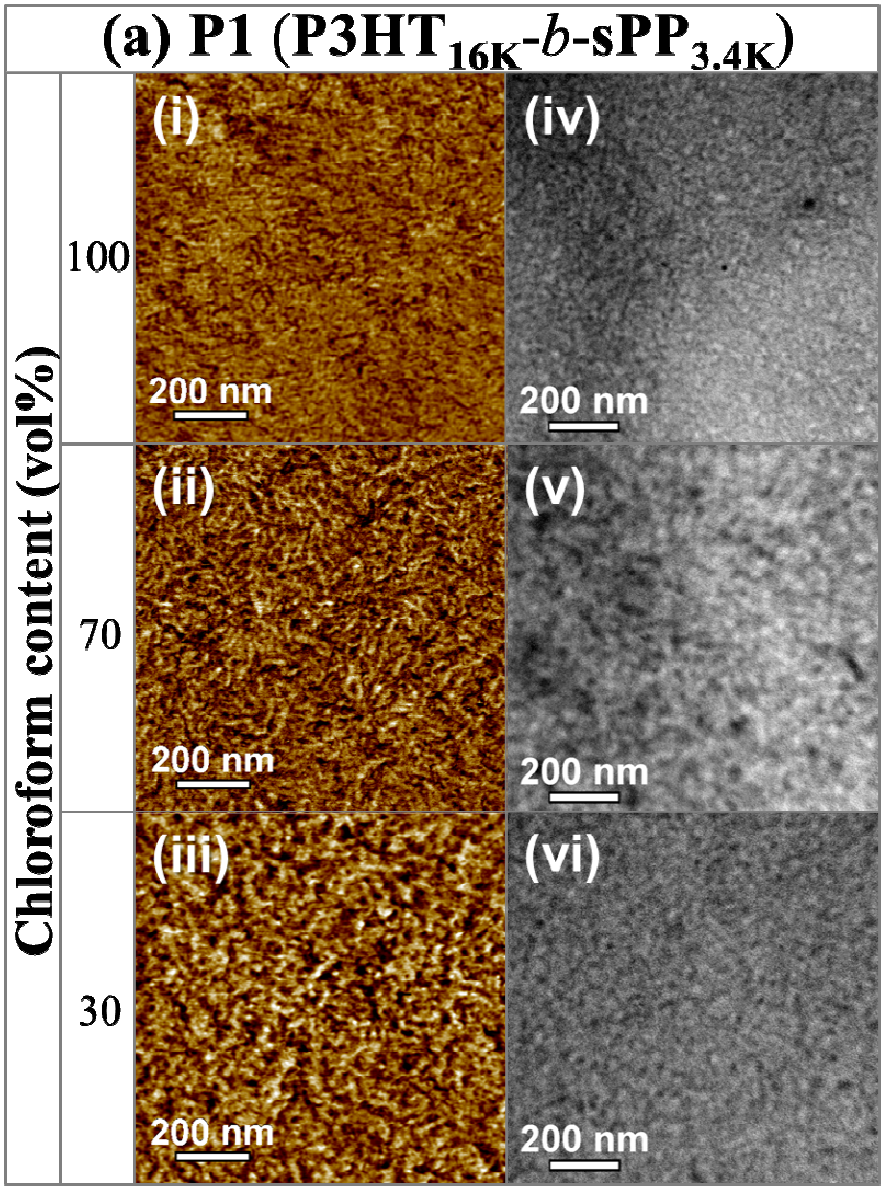

Figure 5(a).

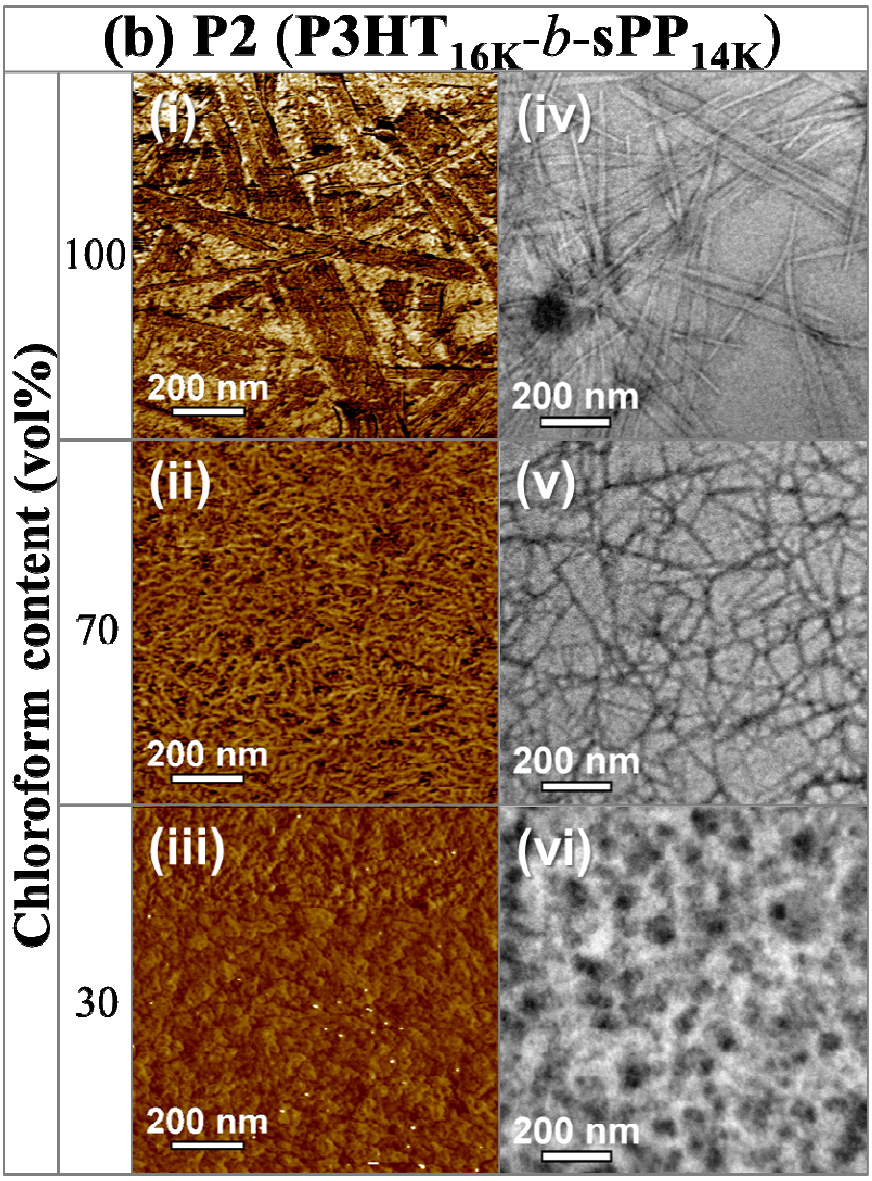

Figure 5(b).

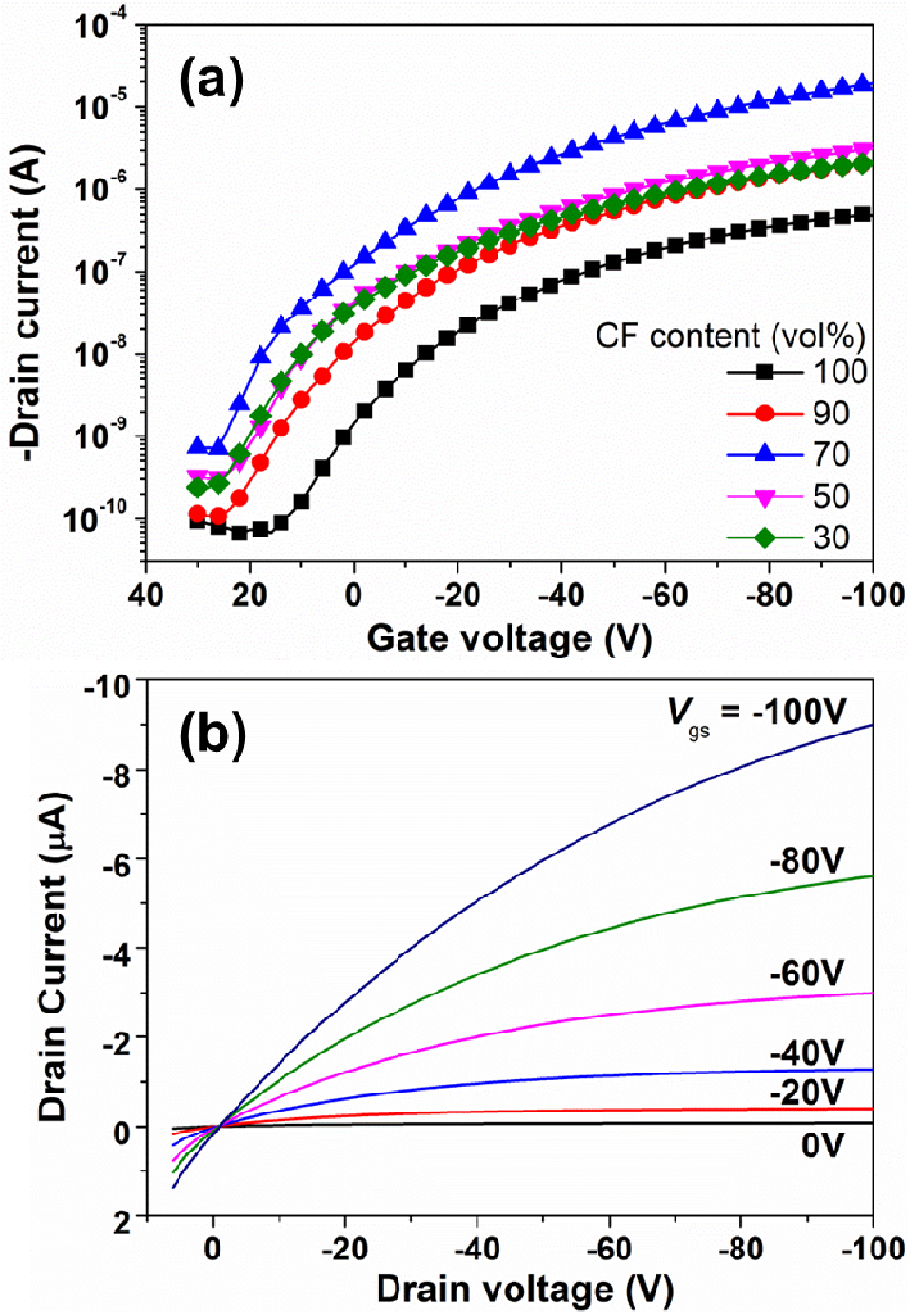

Figure 6.

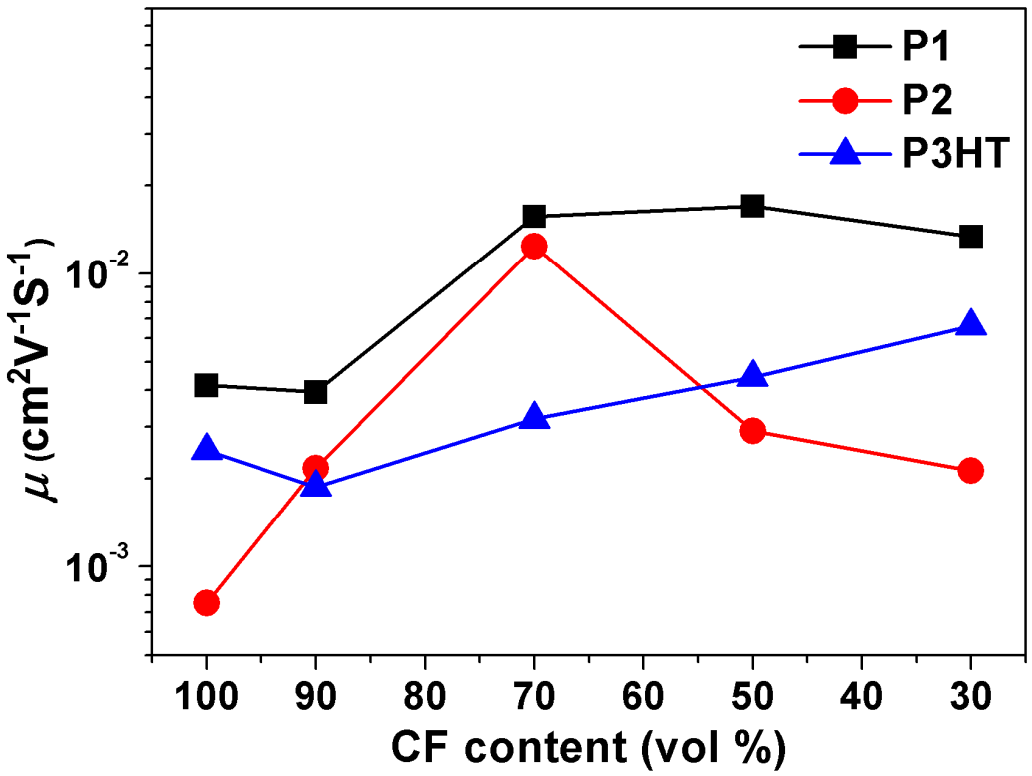

Figure 7.

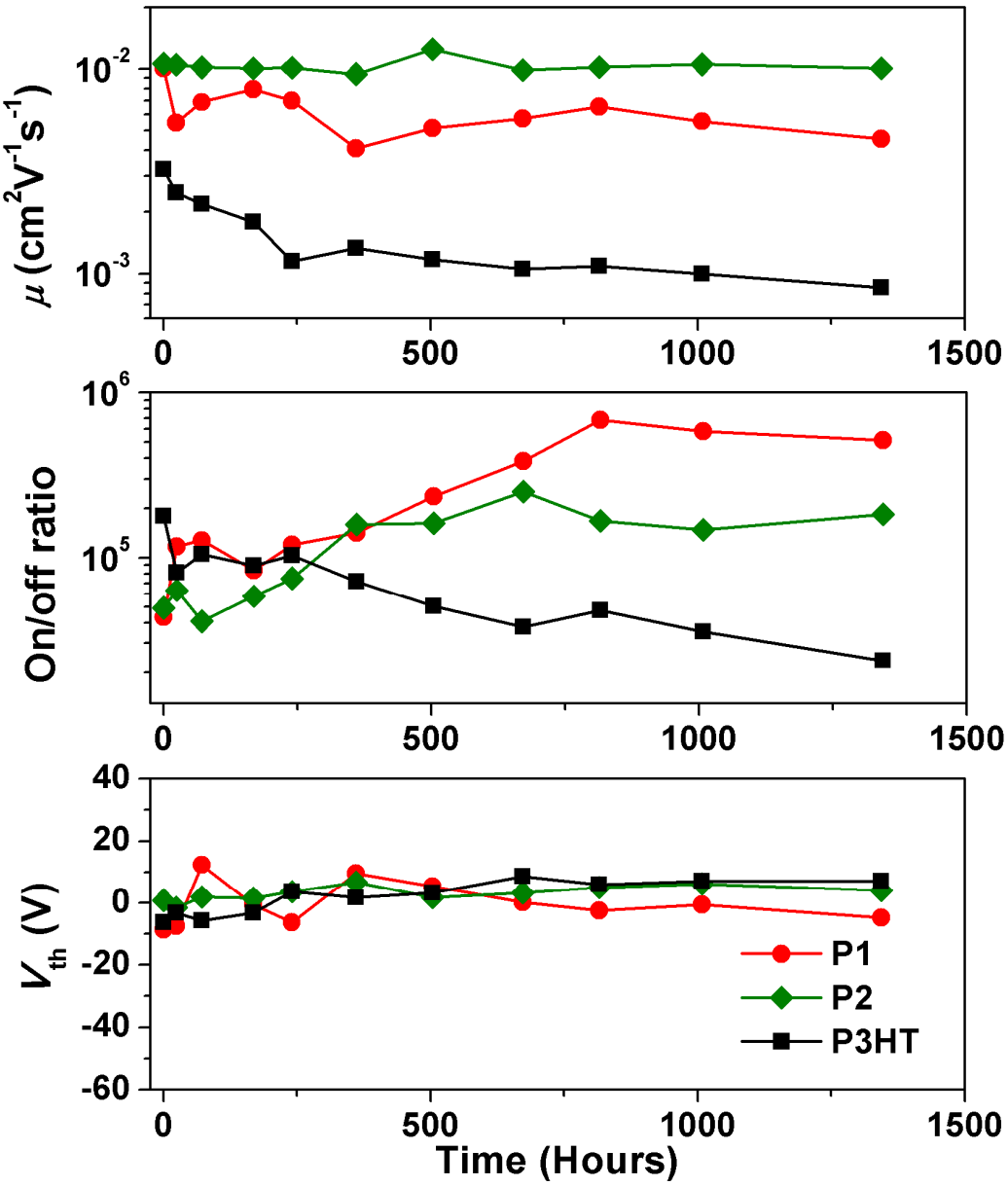

Figure 8.

Table of Contents (TOC)